CONF-9510195-5

Characterizing the Effects of Friction Liner Materials On The Performance of Piezoelectric Motors Using Finite Element Analysis

Kansas City Division

Dr. G. D. Gute and
S. L. Halter

KCP-613-5695

Published October 1995

Prepared Under Contract Number DE-AC04-76-DP00613 for the
United States Department of Energy

AlliedSignal
AEROSPACE

DISCLAIMER

Printed in the United States of America.

This report has been reproduced from the best available copy.

Available to DOE and DOE contractors from the Office of Scientific and Technical Information, P. O. Box 62, Oak Ridge, Tennessee 37831; prices available from (615) 576-8401, FTS 626-8401.

Available to the public from the National Technical Information Service, U. S. Department of Commerce, 5285 Port Royal Rd., Springfield, Virginia 22161.

KCP-613-5695
Distribution Category UC-706

CHARACTERIZING THE EFFECTS OF FRICTION LINER MATERIALS ON THE PERFORMANCE OF PIEZOELECTRIC MOTORS USING FINITE ELEMENT ANALYSIS

Dr. G. D. Gute, University of Missouri, and
S. L. Halter, AlliedSignal Inc., Kansas City Division

Published October 1995

Paper submitted to 66th Shock and Vibration Symposium
October 30-November 3, 1995
Biloxi, MS

AlliedSignal
AEROSPACE

CHARACTERIZING THE EFFECTS OF FRICTION LINER MATERIALS ON THE PERFORMANCE OF PIEZOELECTRIC MOTORS USING FINITE ELEMENT ANALYSIS

Dr. G. D. Gute
University of Missouri
5605 Troost Ave.
Kansas City, Missouri 64110
(816) 235-1284

S. L. Halter
AlliedSignal Inc., Kansas City Division*
2000 East 95th St.
Kansas City, Missouri 64131-3095
(816) 997-4666

ABSTRACT

A finite element model of a Panasonic USM-40D piezoelectric motor's rotor was coupled with a finite element model of the motor's friction liner/rotor so that the frictional interface could be further studied. Results from the model were used to study the affects of various friction liner material properties on motor stall torque. Statistical methods were used to determine the significant friction liner material properties and their interactions. An equation for predicting the stall torque as a function of the significant variables and their interactions was established.

INTRODUCTION

While the traditional electric motor converts electrical energy to mechanical energy through the mutual actions of an electric current and a magnetic field, the piezoelectric motor converts electrical energy into mechanical energy by converting electrically induced vibratory motion into unidirectional motion through frictional coupling.

Although piezoelectric motors have become widely popular in Japan, they have been almost unheard of in the United States and Europe until recently. There are now over 90 U.S. patents for ultrasonic motors and actuators, most of which are owned by the Japanese. Some development has begun in the United States, but most of the U.S. research is focused around piezoelectric ceramic processing and development.

One reason for all this activity is that piezoelectric motors provide a number of distinct advantages over the traditional electric motor. The piezoelectric motor can develop a very large torque per unit volume. Output torques of up to ten times higher than conventional drives of the same volume have been reported [1]. They can be made extremely small and light weight. Motors as small as 1 mm in diameter have been reported [2]. Their operating speed can be

*Operated for the United States Department of Energy under Contract No. DE-ACO4-76-DP00613.

adjusted down to zero if required without the need for gearing, and they maintain an extremely large holding torque when at rest without additional elements and energy supply. These characteristics, as well as their excellent controllability, quick response, and freedom from magnetic noise, make them highly attractive for many applications.

Energy conversion in a piezoelectric motor is a two-stage process. The first process, the conversion of electrical energy into oscillatory bending motion, is usually accomplished through the excitation of piezoelectric elements. Excitation frequencies depend on the specific geometry of the device and the form of excitation -- longitudinal, torsional, or flexural modes of bending -- but are typically between 20 and 150 kHz. The efficiency of this energy conversion process has been estimated to be about 96% [3], but it is dependent upon the specific geometry and the bending mode.

The second energy conversion process in an ultrasonic motor is the conversion of high frequency oscillatory vibration into macroscopic, unidirectional rotary or linear motion via frictional coupling. This process is essentially a vibro-impact system that displays nonlinear dynamics. The efficiency of this energy conversion process has been estimated to be only about 50% [3].

Theoretical estimation of piezoelectric motor performance is difficult, but in general, they offer lower conversion efficiency (< 45%) than electric motors. This lower efficiency can be attributed to a number of factors including the physical design of the stator, the mechanical and piezoelectric properties of the piezoelectric ceramic, the electrical drive circuitry, and the mechanical and frictional characteristics of the materials used for frictional coupling.

In this paper we will explore the frictional interaction between the stator teeth and the friction liner/rotor of a Panasonic USM-40D piezoelectric motor using finite element analysis. A linear motor model of one quarter of the USM-40D piezoelectric motor is proposed. The finite element model is then used to determine the effects of various friction liner material properties on the stall torque of the motor. Statistical analysis techniques are used to determine the significant friction liner material variables and their interactions. Model results are fitted to a quadratic response curve to develop a prediction equation for motor stall torque based on significant friction liner material variables and their interactions.

STATOR/FRICTION LINER CONTACT MODELING

What we are primarily interested in for the use of ultrasonic motors is how much power can be delivered to a load and what the form of the torque-speed curve will take. In order to further understand these two things, we must investigate the interaction between the stator tooth and the friction liner.

Several researchers have investigated this frictional coupling phenomenon. In 1987, Endo and Sasaki [4] reported the results of friction liner tests conducted using a linear ultrasonic motor with a toothless stator and a variety of frictional interface materials. Okumura and Mukohjima [5] and Hosoe [6] reported on wear problems associated with this frictional interface and discussed efforts at improving the efficiency of a Canon ring-type ultrasonic motor. In 1988, Kurosawa and Ueha [7] issued the results of their closed-form analysis of the frictional interface losses, claiming theoretical limits of 70% efficiency for the traveling wave motor. In 1991, Nakamura, Kurosawa, Kurebayasi, and Ueha [8] developed a method of ultrasonic motor testing

based on the motor's transient response, and conducted a number of friction liner tests. In 1992, Maeno, Tsukimoto, and Myake [9] modeled the contact behavior of a ring-type ultrasonic motor using finite element analysis and discovered a stick/slip phenomenon between the stator tooth and the liner material. That same year, Maeno and Bogy [10] went on to study the hydrodynamic bearing effects on the rotor/stator contact. Also, Yoshinobu Imasaka, Hiroshi Yoneno, and Masanori Sumihara [11] published the results of friction liner tests on a number of different material formulations and suggested formulations to maximize motor performance with regards to breaking torque, restarting performance, surface wear, noise generation, and resonant frequency variation. In 1993, Hirata and Ueha [12] proposed a lumped mass equivalent circuit for the calculation of the load characteristics of a traveling wave type ultrasonic motor, and Minotti and Lallement modeled the rotor/stator interaction parameterizing the contact conditions of a nonrigid rotor in terms of the angle of contact. Also, Flynn [13] investigated the contact mechanics of the rotor and the stator using a number of simple interface condition models and discussed the torque/speed trade-off's due to the interpenetration of the stator into the friction liner material.

While the efforts of the researchers discussed above have provided valuable insight into the frictional coupling phenomenon of the ultrasonic motor, few have attempted to tie specific material attributes of the frictional interface materials to the performance characteristics of the motor. A correlation between frictional interface material attributes and motor performance is needed so that interface materials can be selected to optimize ultrasonic motor performance for a particular application.

Some of the researchers discussed above have attempted to study the effects of various interface materials on motor performance experimentally, but experimental results have been, for the most part, inconclusive. Experimental results require many hours of testing and a large number of data points due to motor resonant frequency fluctuations during operation. Resonant frequency fluctuations have been reported by Panasonic [14], Mentesana [15], and Nakamura, Kurosawa, Kurebayashi, and Ueha [8]. They discuss some possible causes of this fluctuation as being related to losses caused by internal heating of the piezoelectric ceramics, fluctuations of the rotor preload during operation, the quality of epoxy bond joints, viscoelastic behavior of the epoxy bond joints, hysteretic material effects in the stator, and the size of the operating load of the motor.

THE FINITE ELEMENT MODEL

For the purpose of this study, we are primarily interested in determining the optimum friction liner material properties to maximize the output torque of the USM-40D ultrasonic motor. A finite element model of the USM-40D is constructed by coupling the finite element model of the motor's stator with a finite element model of the friction liner and rotor as shown in Figure 1.

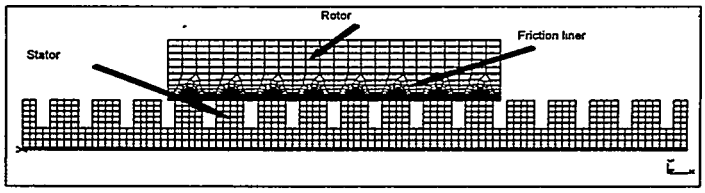

Figure 1: Finite element model used in the stator tooth/friction liner analysis. Stator tooth interactions for one full wavelength (1/4 of the motor) are modeled.

In the model, the rotor is spring loaded against the stator using a theoretical spring with the same spring constant (k=300 lb/in.) as the one used in the Panasonic USM-40D piezoelectric motor. The rotor is restrained in the x-direction but allowed to move up and down in the y-direction to oppose the rotor preload (spring force) as shown in Figure 2.

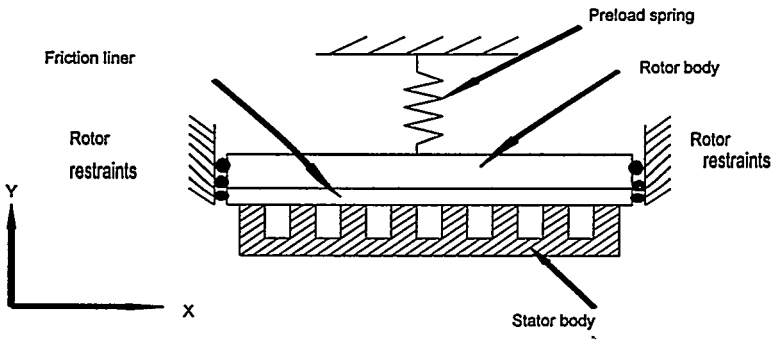

Figure 2: Simple graphic depiction of the finite element model showing how the rotor is restrained.

The stator teeth are forced through their elliptical trajectory, and the frictional interaction between the stator teeth and the friction liner results in an x-directional force being exhibited by the rotor restraints. Since the model is quasi-static, the force exhibited by the rotor restraints must be equal and opposite to the frictional force developed at the stator tooth/friction liner interface, as shown in Figure 3.

By summing the x-directional forces at the rotor restraints, the frictional force developed by the interaction of the stator tooth with the friction liner is obtained. This restraining force is then used as a measure of the output force of the ultrasonic motor. If the stator radius at the location of the teeth is known, this output force can be converted directly to an output torque of the motor. This finite element model is then used to study the effects of varying the Young's modulus, mass density, and Poisson's ratio of the friction liner material along with coefficient of friction and rotor preload on the stall torque of the motor.

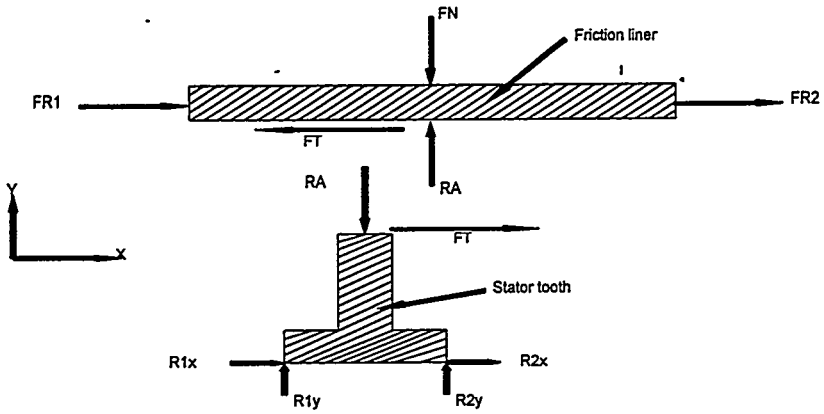

Figure 3: Free-body diagram of the stator tooth and the friction liner. Forces are shown for only one tooth to simplify the diagram.

THE ABAQUS CONTACT MODEL

When two surfaces come in contact, a stress is transmitted across their common surface. If no friction is present at the interface only a normal stress is transmitted across the common surface. However, if friction is present at the contact interface, a normal component and a shear component of stress are transmitted across the common surface. The contact area and the contact stresses must be determined in order to solve the contact problem.

ABAQUS requires the use of special contact elements when solving contact problems. A number of different types of contact elements are available in ABAQUS, but the element type chosen for the ultrasonic motor contact model was the ISL type.

ISL elements are used for modeling contact between two deforming bodies that slide along each other. Contact load transfer occurs between the nodes of the ISL element, which is attached to one deforming body, and a slideline which is attached to the other deforming body. The nodes of the ISL element form the slave surface and slide along the slideline attached to the master surface. For this model, two node ISL elements are positioned on the friction liner (slave surface), and the slideline is positioned on the top of each stator tooth (master surface). These elements provide for output of the shear stress at the frictional interface (S12), the normal stress or contact pressure at the contact interface (S11), the separation of the surfaces normal to the slide line (E11), and the accumulated relative tangential displacement of the contact surfaces (E12).

The contact model uses the classical Coulomb friction model which assumes that the surfaces in contact will not slide over one another as long as the shear stress magnitude is less than the coefficient of friction times the contact pressure between the two surfaces. When the shear stress reaches a critical value, τ^{o}, the two surfaces in contact will slide along each other. The value of this critical stress, τ^{o}, is equal to the coefficient of friction, μ, times the contact pressure, P. Often, the shear stress is lower during slipping than the value required to initiate slip. In this case, a coefficient of kinetic friction is often introduced. However, the friction

model used in this analysis provides for only a single value of μ for each possible contact surface.

Contact models require the imposition of constraints between the points that are in contact. ABAQUS uses the Lagrange multiplier method for the imposition of the contact constraints. The Lagrange multipliers are defined as internal variables and are not apparent to the user, except when equation solver problems occur. For each potential contact point, the contact condition is described by the single, nonlinear, inequality constraint:

$$h(u^1, u^2, u^3, \ldots) \geq 0$$

where h is the "clearance" between the points, and u^n are the kinematic degrees of freedom. If $h \leq 0$, the contact constraints are imposed, and the contact area, the contact pressure, and the shear stresses are calculated. No contact constraints are imposed if $h > 0$.

The use of contact elements automatically invokes the assumption of large displacement, small strain theory, or Green's strain theory in ABAQUS. Green's strain theory suggests that the strain, $f(\lambda)$, is defined by:

$$f(\lambda) = \frac{1}{2}(\lambda^2 - 1)$$

where λ is termed the stretch ratio, and is defined as:

$$\lambda = \frac{dl}{dL}$$

where dL is the initial distance between the nodes of the structure and dl is the current distance between the nodes of the structure. Thus, the Green's strain matrix can be established once the deformation gradients are established without the need to solve for the principle directions, which makes Green's strain computationally attractive.

RESULTS

Since the frictional drive force of the stator tooth depends upon the contact pressure between the tooth and the friction liner, the difference in the contact surface areas between that of the actual USM-40D stator tooth and the stator tooth of the proposed finite element contact model must be considered if the frictional output forces from each are to be compared. The equivalent contact surface area, A_e, of the USM-40D is 0.15168 square inches (0.00474 x 32). The equivalent contact surface area, A_{fe}, of the finite element model is .48 square inches (0.06 x 8).

By setting the equivalent contact pressure of the finite element model, P_{fe}, equal to the equivalent contact pressure of the USM-40D, P_e, some comparison can be made between the output force results. Since the "as received" preload, F, for the USM-40D was determined to be 6 lbs [15], and the equivalent contact pressure, $P_e = F/A_e$, the equivalent contact pressure is 39.56 psi. Setting $P_e = P_{fe}$, the equivalent preload force for the finite element model is 18.98 lbs.

Thus, a 6 lb preload force for the USM-40D is equivalent to an 18.98 lb preload force for the finite element contact model, a ratio of about 3 to 1 for the finite element model.

The starting torque for the USM-40D is 500 gf-cm or 6.945 ounce-inches. Converting the starting torque value to a linear equivalent load, F_l, at the radius of the stator teeth (r=.465 in.) we find the equivalent load, F_l= 0.93355 lb. The actual tooth thickness for the USM-40D stator tooth is 0.079 inches. Dividing the equivalent starting torque load, F_l, by the tooth thickness (0.079) gives the equivalent normalized load, F_{ln}=11.817 lbs/inch.

The results of the finite element contact model, using a friction liner material with a Young's modulus of 136000 psi, a coefficient of friction of 0.22, and a rotor preload of 18 lbs, indicate an average output force of 3.07 lbs. Since only one fourth of the motor is modeled, we would expect the model to predict an average output force of 12.28 lbs. for the USM-40D. Thus, the model output force prediction appears to be within about 4% of the USM-40D rated output force.

Figure 4 shows the effect of the stator tooth interactions with the friction liner when the stator is forced through its elliptical trajectory. The force values are negative, since the rotor restraints are applying a force in the negative x-direction to keep the rotor from moving. This figure indicates that the drive force (frictional force) is a minimum as the primary drive function is transferred from one tooth to the other. It also indicates that the total output force is not constant, but fluctuates as the primary driving function transfers from one tooth to the other. Thus, it is the combined interaction of the stator teeth with the friction liner material that creates the total output force.

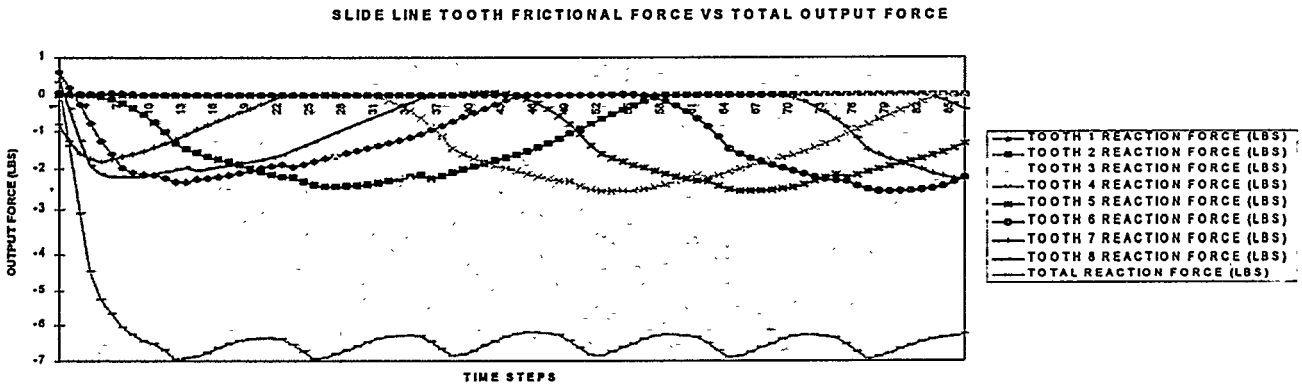

Figure 4: The frictional forces generated by the stator teeth when a PPO Polycarbonate friction liner is used, E=374500 psi, μ=.3, and the rotor preload is 24 lbs.

Additional analysis of the frictional interface indicated that the maximum drive force occurrs when the amount of preload supported by each tooth is a maximum and that the maximum output force occurs at the point where a stator tooth is in complete contact with the friction liner surface.

From Figure 4, we see that the total output force of the motor is not a constant value, but fluctuates as the stator teeth interact with the friction liner material. Since we are primarily interested in studying the effects of different friction liner materials on the output force of the model, the average output force was chosen as the figure of merit for each friction liner material. Thus, an average output force for the time steps on each computer simulation was calculated.

Figure 5 compares the average output force of the model with both a HMW polyethylene and PPO polycarbonate friction liner material for a given rotor preload and coefficient of friction. Figure 5 indicates a complex relationship between rotor preload, coefficient of friction, Poisson's ratio, and density of the friction liner material. Although the figure indicates a general increase in model average output force as the coefficient of friction, Young's Modulus, and rotor preload increase, a better understanding as to how these variables and their interactions affect the average output force of the motor is needed so that interface materials can be selected to optimize piezoelectric motor performance for a particular application.

Box-Behnken, Four-Level Full Factorial, and Central Composite experimental design techniques are used to identify the model variables (Young's Modulus (E), rotor preload or normal force (F), coefficient of friction (μ), liner material density (ρ), and liner Poisson's ratio (γ)) and the variable interactions statistically significant to the average output force prediction of the model. Data ranges are chosen for each model variable. The Young's Modulus of the friction liner material ranges from 15,000 to 1,000,000 psi, the rotor preload ranges from 1 to 36 lbs, the coefficient of friction ranges from .1 to .5, the Poisson's ratio ranges from .1 to .5, and the material density ranges from 0.5×10^{-4} to 7.3×10^{-4} slugs/in.^{3}.

The effect of the five model variables and their interactions on the model's predicted average output force is determined using regression analysis on the data from all three experimental designs. The significant variables are identified to be the Young's Modulus (E) of the friction liner material, the coefficient of friction (μ) between the friction liner and the stator tooth, and the normal force (F). The significant variable interactions are determined to be the Young's Modulus with the coefficient of friction, the Young's Modulus with the normal force, the coefficient of friction with the normal force, and the Young's Modulus with itself.

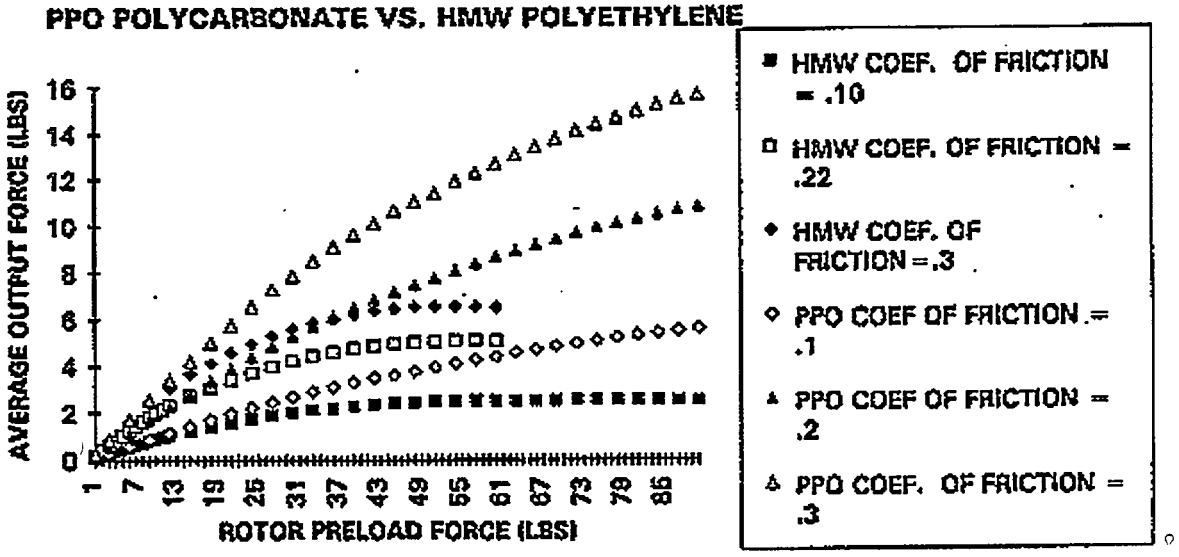

Figure 5: The average output force of a PPO Polycarbonate friction liner vs. a friction liner of HMW Polyethylene for a given preload and coefficient of friction.

The data points for each of the significant variables and their interactions are then fitted to a quadratic response curve so that an equation to predict the model output force as a function

of the significant variables and their interactions is developed. The prediction equation for the average output force of the model is:

$$AOF=5.23+2.20Y+3.59F+3.59N+1.48YF+2.24YN+2.41FN-2.44Y^2$$

where AOF, Y, F, and N represent the average output force of the model, the Young's Modulus, the coefficient of friction, and the normal force, respectively. For use in the prediction equation given above, the values of Y, F, and N must be scaled according to Table I.

TABLE I. SCALING OF PARAMETERS

PARAMETER	ACTUAL VALUE		SCALED VALUE	
YOUNG'S MODULUS (Y)	1,000,000	15,000	+1	-1
COEFFICIENT OF FRICTION (F)	0.5	0.1	+1	-1
NORMAL FORCE (N)	36	1	+1	-1

Statistically, the average output force (AOF) prediction given by the equation listed above is within +/-2.5 lbs of the computer-simulated value for the average output force, with a 95% likelihood.

CONCLUSIONS

One quarter symmetry of a Panasonic USM-40D piezoelectric motor is modeled as a linear motor model using finite element analysis. The stall torque prediction of the finite element contact model is very close (within 4%) to the manufacturer's published value of stall torque for the USM-40D piezoelectric motor when the data is normalized for differences in the frictional contact areas. This close correlation allows us to use this model to further study the frictional interface. Our analysis indicates that it is the combined interactions of several stator teeth that produce the output torque of the piezoelectric motor, and thus, the output torque of the piezoelectric motor is not constant, but fluctuates as the primary driving function transfers from one tooth to the other. The initial contact between the stator tooth and the friction liner occurs at the sharp edge of the stator tooth, and the maximum individual driving force for each tooth occurs when the tooth has the largest contact area with the friction liner.

Statistical experimental design techniques were used to determine the significant frictional interface material variables and the variable interactions for the model. The significant model variables were determined to be the Young's Modulus of the friction liner material (E), the coefficient of friction (μ) between the friction liner and the stator tooth, and the rotor preload (F). The significant variable interactions were determined to be the Young's Modulus with the

coefficient of friction, the Young's Modulus with the normal force, and the Young's Modulus with itself.

The data points for significant variable and variable interactions were then fitted to a quadratic response curve to develop an equation for the model output force as a function of the significant variables and their interactions. Using this equation, the frictional interface parameters can be selected to optimize motor performance for a particular application.

REFERENCES

1. G. Schaedebrodt, "The Piezo Traveling Wave Motor," Design Engineering, pp. 36-41, January 1991.

2. A. M. Flynn, "The Scoop on Ultrasonic Motors in Japan," December 1991.

3. Sadayki Ueha, "Present State of the Art of Ultrasonic Motors," Japanese Journal of Applied Physics, Vol. 28, Supplement 28-1, pp. 3-6, 1989.

4. Akira Endo and Nobutoshi Sasaki, "Investigation of Frictional Material for Ultrasonic Motor," Japanese Journal of Applied Physics, Vol. 26, Suppl. 26-1, pp. 191-193, 1987.

5. I. Okumura and H. Mukohjima, "A Structure of Ultrasonic Motor for Auto Focus Lenses," Proceedings of Motor Control, September 1987.

6. Kazuya Hosoe, "An Ultrasonic Motor for Use in Autofocus Lens Assemblies," Techno, pp. 36-41, May 1989, in Japanese.

7. M. Kurosawa and S. Ueha, "Efficiency of Ultrasonic Motor Using Traveling Wave," Journal of the Acoustic Society of Japan, Vol. 44, No. 1, pp. 40-46, 1988, in Japanese.

8. Kentaro Nakamura, Ninoru Kurosawa, Hisayuki Kurebayashi, and Sadayuki Ueha, "An Estimation of Load Characteristics of an Ultrasonic Motor by Measuring Transient Responses," IEEE Transactions on Ultrasonics, Ferroelectrics, and Frequency Control, Vol. 38, No. 5, September 1991.

9. Takashi Maeno, Takayuki Tsukimoto, and Akira Miyake, "Finite Element Analysis of the Rotor/Stator Contact in a Ring-Type Ultrasonic Motor," IEEE Transactions on Ultrasonics, Ferroelectrics, and Frequency Control, Vol. 39, No. 6, November 1992.

10. Takashi Maeno and David B. Bogy, "Effect of the Hydrodynamic Bearing on Rotor/Stator Contact in a Ring-Type Ultrasonic Motor," IEEE Transactions on Ultrasonics, Ferroelectrics, and Frequency Control, Vol. 39, No. 6, pp. 675-682, November 1992.

11. Yoshinobu Imasaka, Hiroshi Yoneno, and Masanori Sumihara, "Ultrasonic Motor," U.S. Patent 5,150,000, September 22, 1992.

12. H. Hirata and S. Ueha, "Characteristics Estimation of a Traveling Wave Type Ultrasonic Motor," IEEE Transactions of Ultrasonics, Ferroelectrics, and Frequency Control, Vol. 40, No. 4, pp. 402-406, July 1993.

13. A. M. Flynn, "Torque Production in Ultrasonic Motors," MIT Artificial Intelligence Laboratory, January 1994.

14. Panasonic Technical Reference, "Ultrasonic Motor," Electric Motor Division, Matsushita Electric Industrial Co., Ltd.

15. Mentesana, C. P., "Optical Stronglink Development and Piezoelectric Motor Evaluation," AlliedSignal Inc., Kansas City Division, May 1992.

BIBLIOGRAPHY

ABAQUS Standard User's Manual II, Version 5.2, Hibbitt, Karlson, and Sorensen, Inc., 1992.

ABAQUS Theory Manual, Version 5.2, Hibbitt, Karlson, and Sorensen, Inc., 1992.

"IDEAS Finite Element Modeling User's Guide," Structural Dynamics Research Corp., 1990.

S. L. Halter, Master's Defense, "Characterization of Friction Liner Materials For Piezoelectric Motors Using Finite Element Analylsis," University of Missouri-Columbia, December 1994.